Study on reservoir characteristics, pore-throat structure, and origin of tight oolitic reservoirs: A case study of Triassic Feixianguan Formation, NE Sichuan Basin, SW China

Guanxiong Ren[1,2]*, Qirong Qin[1,2], Qiang Zhang[3], Yanbo Guo[4] and Zhaoyang Ye[4]

[1]School of Geosciences and Technology, Southwest Petroleum University, Chengdu, China, [2]State Key Laboratory of Oil and Gas Reservoirs Geology and Development Engineering, Chengdu, China, [3]PetroChina Southwest Oil and Gas Field CDB Operating Company, Dazhou, China, [4]Chongqing Gas Mine, PetroChina Southwest Oil and Gas Field Company, Chongqing, China

The origin and pore-throat structure of different lithofacies are key issues in exploration and development of tight oolitic reservoirs. Based on core and thin section observation, four types of lithofacies can be recognized in the Feixianguan Formation oolitic reservoir: 1) oolitic limestone with intergranular pores (Lithofacies A), 2) oolitic limestone with mold pores (Lithofacies B), 3) oolitic dolostone (Lithofacies C), and 4) silty crystalline dolomite and fine crystalline dolostone (Lithofacies D). The subsurface core samples from the different lithofacies were studied using mercury injection, 3D CT scanning, and nuclear magnetic resonance, indicating that Lithofacies D possesses the best pore-throat structure and reservoir connectivity. The pore-throat structure of Lithofacies C is very similar to that of D, but the heterogeneity is much stronger. By comparison, the pore-throat structure of Lithofacies A and B is relatively poor. Although the pore heterogeneity of Lithofacies B is weaker than that of Lithofacies A, there is no effective throat connection in Lithofacies B. On the basis of oolitic shoal deposition, the factors controlling the origin of different lithofacies are meteoric freshwater leaching and then dolomitization. Meteoric freshwater leaching dominates the origin of Lithofacies B but does not affect the origin of Lithofacies C. Lithofacies C is jointly controlled by seepage-reflux and hydrothermal dolomitization fluids. The origin of Lithofacies D is only controlled by seepage-reflux dolomitization. Some other diagenesis effects may also have an impact on petrophysical properties of different lithofacies, but they do not play a decisive role in the origin of different lithofacies.

KEYWORDS

tight oolitic reservoir, dolomitization, formation mechanism, controlling factors, lithofacies, Feixianguan Formation

1 Introduction

Oolitic shoal commonly possesses high primary interparticle porosity, as well as large cumulative thickness, and wide distribution range (Enos and Sawatsky, 1981; Schmoker and Hester, 1986). Therefore, oolitic shoal has always been the ideal target of oil and gas exploration since 1960s (Akin and Graves, 1969). At present, successful exploration cases have been obtained in the oolitic reservoir of the Carboniferous, Permian, Triassic, and Jurassic periods throughout the world, such as Walker Creek Oilfield in Arkansas (Swirydczuk, 1988; Bliefnick

and Kaldi, 1996), Big Bow and Sand Arroyo Creek Oilfield in southwest Kansas (Qi et al., 2007), De Wijk and Wanneperveen Oilfield in the Netherlands (Palermo et al., 2008), South Pars Gas field and Balal Oilfield in Iran (Esrafili-Dizaji and Rahimpour-Bonab, 2014; Ebrahim et al., 2018), Villeperdue Oilfield in Paris Basin of France (Granier, 1995), and Puguang Gas field in Sichuan Basin of China (Li H et al., 2020; Li Y et al., 2020).

However, an oolitic reservoir shows strong heterogeneity in pore type, porosity, permeability, and pore-throat structure, which has great influence on exploration and development deployment. Swirydczuk (1988) first proposed that original mineralogy and diagenesis jointly control permeability and pore type in the oolitic reservoir. Bliefnick and Kaldi (1996) used high-pressure mercury injection (MICP) to compare the differences in pore structure of different lithofacies in oolitic limestone reservoirs. It is considered that mechanical compaction and calcite cementation are the negative factors of pore-throat structure, and the higher the degree of sorting, the better the pore structure. However, Makhloufi et al. (2013) argued that early compaction, with the development of grain interpenetration, permits better connectivity in the pore-throat structure, leading to better reservoir properties. Other researchers also noticed the differences in reservoir characteristics of different lithofacies in oolitic reservoirs (Palermo et al., 2008; Esrafili-Dizaji and Rahimpour-Bonab, 2014), but the research objects focus on geometry and distribution of oolitic shoal deposits (Qi et al., 2007; Qiao et al., 2016) and diagenetic evolution of porosity in different lithofacies (Esrafili-Dizaji and Rahimpour-Bonab, 2014; Li et al., 2017; Morad et al., 2019). At present, previous studies on pore-throat structure of oolitic reservoirs are rare, and only a few studies have discussed pore structure using MICP without lithofacies classification (Wang et al., 2018; Zhou et al., 2019). Lack of detailed comparison of pore-throat structure differences between different lithofacies leads to insufficient discussion on controlling factors.

The proven reserves of oolitic gas reservoirs in the Triassic Feixianguan Formation around the Kaijiang–Liangping Trough in the northeastern Sichuan Basin have exceeded $5,000 \times 10^8$ m³ (Zou et al., 2011). With the deepening of exploration and development, previous studies have illustrated that the oolitic reservoirs of different wells are composed of one lithofacies or multiple lithofacies combinations (Wang et al., 2018; Gu et al., 2021), and the gas production of each well varies greatly. The unclear understanding of reservoir characteristics, pore-throat structure, and controlling factors has become the decisive factor restricting the next exploration and development.

In this study, we first classify the lithofacies of oolitic reservoirs according to the macro–micro petrological characteristics. Then, pore type, throat type, and petrophysical property of different lithofacies are discussed using 3D CT scanning, low-field nuclear magnetic resonance (NMR), MICP, and scanning electron microscopy (SEM) (Fan et al., 2020). Finally, based on cathodoluminescence (CL), stable isotope, and rare Earth element (REE) data, factors controlling the origin of different lithofacies are studied, and a sedimentary-diagenetic evolution model is established. This study helps guide the further exploration and development of oolitic reservoirs.
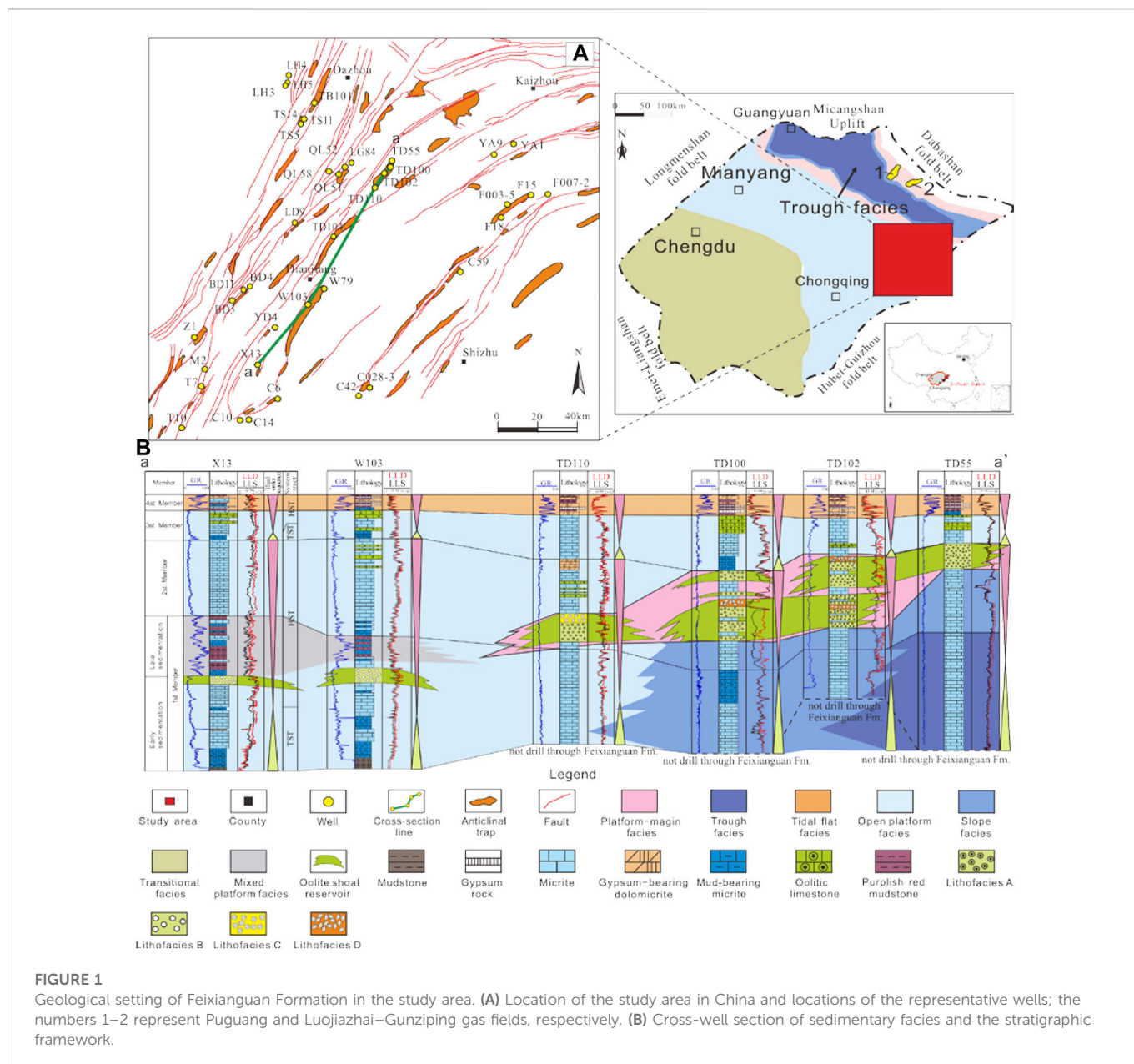
2 Geological background

The Sichuan Basin lies on the relatively northwestern side of the Yangtze platform and is surrounded by the Daba and Micang

mountains in the north, the Longmen Mountains in the west, Lou Mountain and the Daliang Mountains in the south, and Qiyue Mountain in the east (Wei et al., 2018; Jin et al., 2020; Ren et al., 2022).The basin in its geological history has experienced both tectonic evolution stages featuring tensile stress from the Sinian to Middle Triassic and horizontal compressive stress from the Late Triassic to Quaternary (Wang and Jin, 2002; Liu et al., 2011; Li et al., 2019a). Furthermore, it is divided into six tectonic cycles of Yangtze, Caledonian, Hercynian, Indosinian, Yanshan, and Himalayan (Deng, 1992; He et al., 2011). Based on the regional structural characteristics, the present structural features, and the previous research results, the basin is divided into three structural zones by the Huayingshan and Longquanshan faults, and subdivided into six secondary structural zones, namely, fault–fold belts of high steep in eastern Sichuan, low steep in southern Sichuan, low gentle in southwestern Sichuan, gentle in central Sichuan, gentle in northern Sichuan, and low gentle in western Sichuan (Zhou et al., 2016; Li et al., 2019a).

The study area is located in eastern Sichuan Basin (Figure 1A). Due to the combined effects of the "Emei" taphrogenesis and the formation and evolution of the Micangshan Fault Zone and the Guangwang Basin in the north, the study area is in the extensional tectonic setting during the Late Permian–Early Triassic, forming the Kaijiang–Liangping Trough (Xing et al., 2017). The trough is formed during the early Changxingian (Late Permian) due to rapid basement subsidence associated with the "Emei" taphrogenesis (Tan et al., 2012). As a result, a trough-platform sedimentary pattern comprising open platform facies, platform-margin facies, slope facies, ocean trough (basin) facies, and so on existed in both east and west sides of the trough (Zou et al., 2011). With the filling of sediments into the trough, the platform-margin facies gradually migrated to the center of the trough (Gu et al., 2021). Until the third member of Feixianguan Formation, the study area evolved into an open platform facies, which mainly consists of intra-platform oolitic shoal and inter-shoal sediments (Gu et al., 2020). At the end of the Feixianguan deposition (sedimentary period of the fourth member), the evaporation platform facies dominates the study area, which is comprised of gypsum rocks, gypsum-bearing dolomicrite, and mudstone (Figure 1B). Based on the evolution of sedimentary facies and lithology, the Feixianguan Formation can be divided into four members, namely, the first member (T_1f^1), the second member (T_1f^2), the third member (T_1f^3), and the fourth member (T_1f^4) (Figure 2).

3 Samples and methods

The results obtained by the comprehensive study on Feixianguan Formation tight oolitic reservoir were based on core analysis data from 12 cored wells, including TS5, TS11, TS14, TD110, TD102, and TD100 (Figure 1A). To ensure the reliability of this study, samples should be collected and selected in accordance with the following principles: 1) samples shall not be collected from the development parts such as structurally crushed and weathered zones; 2) the structure and state of the sample should be collected as undamaged as possible. The thin sections of drilling cuttings were prepared from the non-cored wells, in order to establish a complete lithology column. First, all core samples involved in the experiments were used for thin sections and SEM analysis individually. The polarized light microscope, CL, and SEM

FIGURE 1
Geological setting of Feixianguan Formation in the study area. **(A)** Location of the study area in China and locations of the representative wells; the numbers 1−2 represent Puguang and Luojiazhai−Gunziping gas fields, respectively. **(B)** Cross-well section of sedimentary facies and the stratigraphic framework.

were used to classify lithofacies. In addition to these studies, two core plugs and one full-diameter core sample were drilled from different lithofacies. Under the test conditions of an injection pressure of 50 MPa and confining pressure range of 0–100 MPa, the porosimeter–permeameter HKGP-3 was used to determine porosity and permeability of core plug samples. Then, the core plug samples were fully saturated with brine. The NMR T_2 spectrum of the core plug samples was acquired by using NUMAG's C12–010V low-field NMR spectrometer under 100% water saturation (Shen et al., 2019; Li 2022). A 3D CT scanning of core samples was then performed using a nanoVoxel-4000 3D X-ray microscope (XRM). Finally, the core plug samples were tested using MICP. The capillary pressure curves and the histogram graphs of the pore-throat radius were obtained (He et al., 2021; Kang 2021; Li H et al., 2022; Li J et al., 2022). Meanwhile, the critical parameters are the following: threshold pressure (P_{cd}), median radius (r_{50}), maximum throat radius (r_{max}), maximum mercury saturation (S_{max}), and mercury extrusion efficiency (E_w).

The remaining samples were used to select fresh sections by avoiding calcite veins and organic matter and grounded to 200 mesh size for rare Earth element (REE) and carbon–oxygen isotope analysis. REE (n = 25 samples) measurements were carried out by inductively coupled plasma-mass spectrometry (ICP-MS). Considering the relationship between carbonate diagenetic fluids and normal seawater, this study selected REE content of seawater published by Kawabe et al. (1998) as the standard. Because REE content of seawater is very low, the REE content of seawater is magnified by 10^4 times before standardization. Eu, Ce, and Pr anomaly values were calculated as follows: $\delta Ce=2Ce_N/(La_N+Pr_N)$; $\delta Eu=2Eu_N/(Sm_N+Gd_N)$; $\delta Pr=2Pr_N/(Ce_N+Nd_N)$ (Shields and Stile, 2001).

The samples for isotopic analysis were microdrilled from the cores. Stable isotopes ($\delta^{18}O$ and $\delta^{13}C$) (n = 48 samples) of different rock fabrics were carried out by using the carbonate reaction method. These test samples reacted in the phosphoric acid bath method at 90℃, and

FIGURE 2
Generalized stratigraphy and tectonic history of the study area (modified from Hao et al., 2008). Sym, symbol.
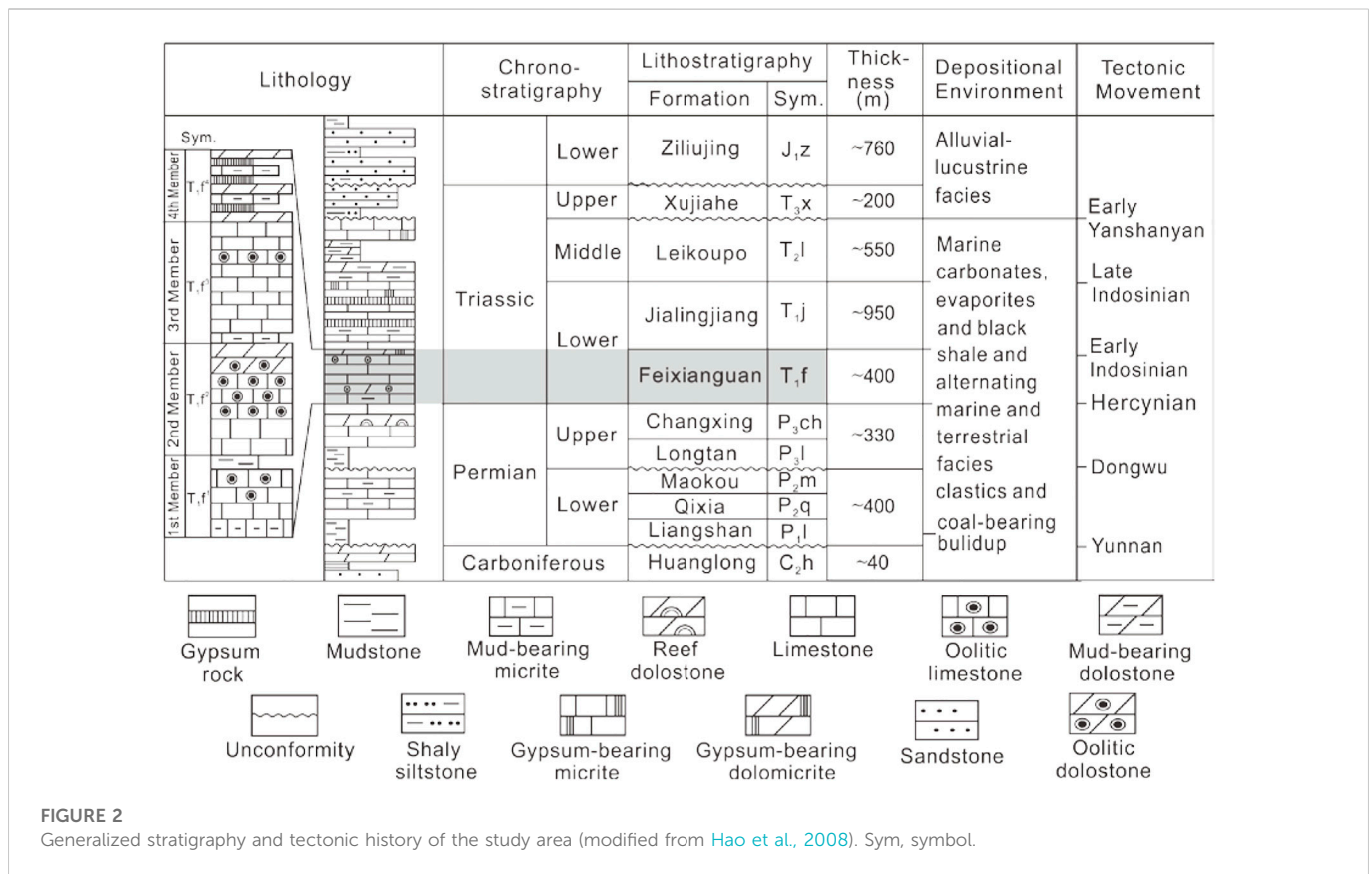
the CO_2 generated was examined using Elementar IsoPrime GC5. Standard isobaric corrections were adopted, while strontium was separated using the Eichrom Sr-Spec resin and measured on a Triton Plus thermal ionization mass spectrometer. All stable isotope data are converted to permille (‰) relative to Vienna Pee Dee Belemnite (VPDB) and corrected by fractionation factors supplied by Fairchild and Spiro (1987). Precision of the $\delta^{18}O$ and $\delta^{13}C$ ratio data is greater than ±.1‰.

4 Results and discussion

4.1 Reservoir characterization of tight oolitic reservoirs

4.1.1 Lithofacies, pore, and throat types

The rock fabrics, depositional structure, and diagenesis of carbonate reservoirs are extremely complex, which lead to complexity in the reservoir space (Guo et al., 2016; Kiani et al., 2021; Abraham-A et al., 2022; Forstner and Laubach, 2022). Typically, the primary pore types are hard to preserve through the late-stage diagenetic environment. Therefore, carbonate reservoirs often possess the characteristics, such as abrupt changes in lithology, various pore types, and unpredictable petrophysical properties. Based on observation of cores and thin sections, the lithofacies of the oolitic reservoir in Feixianguan Formation were classified into four types, namely, Lithofacies A, Lithofacies B, Lithofacies C, and Lithofacies D.

Lithofacies A is oolitic limestone featured by gray colors in the core (Figure 3A). Microscopically, Lithofacies A is composed of ooids and sparry calcite cement (Figure 3B), and the size of each ooid ranged from 500 μm–900 μm and was fabric-selectively replaced by very fine crystalline dolomite (Figure 3C). The main pore type of Lithofacies A is intergranular pores (100–240 μm in diameter) developing between ooids (Figure 3C). The intergranular pores are mainly connected by the tube-shaped throat (50 μm–80 μm in diameter) (Figure 3D).

Lithofacies B is oolitic limestone featured by greyish white color in the core (Figure 3E). Microscopically, most of the ooids in Lithofacies B are fabric-selectively dissolved (Figure 3F), but outermost concentric laminations are well-preserved (Figures 3G, H). The only pore type of Lithofacies B is mold pore (250–500 μm in diameter), and the throat is not developed (Figure 3H).

Lithofacies C is oolitic dolostone featured by white color in the core (Figure 3I). Microscopically, Lithofacies C is composed by subhedral silty crystalline dolomite (Figure 3J) and is characterized by signs of shadowy ooid outlines due to intense dolomitization (Figure 3K). The major pore type of Lithofacies C is intergranular dissolution pore (250 μm–500 μm in diameter) connected by a necking throat (Figure 3L). Very often, the difference between the pores and throats does not become obvious, and this necking throat mainly appears in the intergranular dissolution pores (Figure 3L).

Lithofacies D is oolitic dolostone composed of euhedral silty crystalline dolomite and fine crystalline dolomite (Figures 3M, N). The pore type of Lithofacies D is the intercrystalline pore (100 μm–150 μm in diameter) connected by a flaky throat (15 μm–40 μm in diameter) (Figures 3O, P).
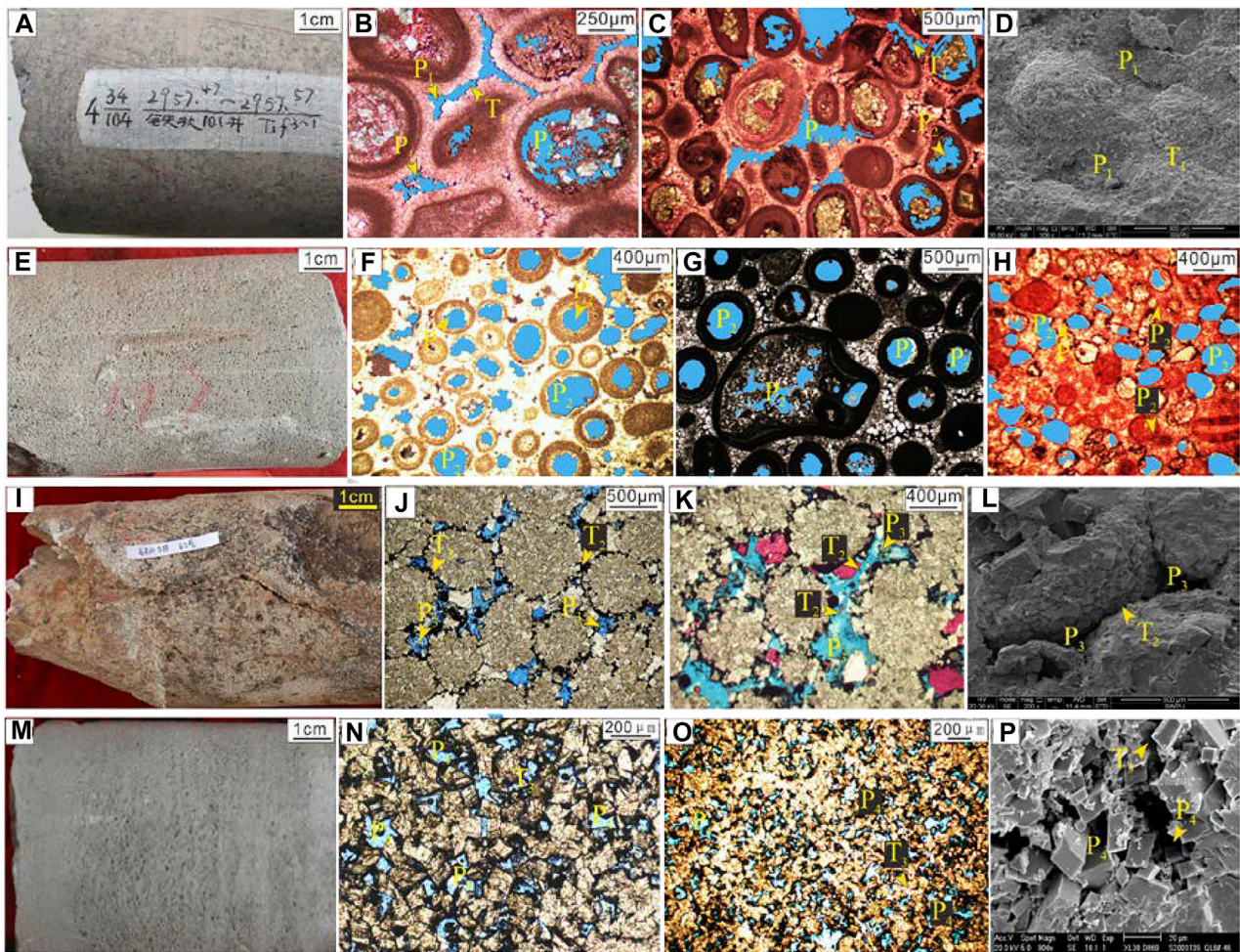
FIGURE 3
Petrological characteristics of different lithofacies in Feixianguan Formation tight oolitic reservoir. **(A)** Intergranular pores (P_1) present as clearly visible pinholes in the drill core, Lithofacies A, Well TB101, 2957.47 m−2957.57 m; **(B)** several intergranular pores (P_1) are connected through tube-shaped throats (T_1), Lithofacies A, Well TB101, 2,956.84 m (PPL); **(C)** intergranular pores (P_1) are connected through tube-shaped throats (T_1), Lithofacies A, Well TD110, 3,457.3 m (PPL); **(D)** intergranular pores (P_1), Lithofacies A, Well TD110, 3,457.3 m (SEM); **(E)** mold pores (P_2) without throats, Lithofacies B, Well C10; **(F)** mold pores (P_2), Lithofacies B, Well C14, 1,678.33 m (PPL); **(G)** mold pores (P_2), Lithofacies B, Well C10 (PPL); **(H)** mold pores (P_2), Lithofacies B, Well X13, 3,297.94 m (PPL); **(I)** intergranular dissolution pores (P_3) present as clearly visible pinholes in drill cores, Lithofacies C, Well TS5, 2,863.32 m; **(J)** intergranular dissolution pores (P_3) are connected by the necking throat (T_2), Lithofacies C, Well TS5, 2,853.36 m (PPL) (Wang et al., 2018); **(K)** intergranular dissolution pores (P_3) are connected by the necking throat (T_2), Lithofacies C, Well TS5, 2,867.34 m (PPL); **(L)** intergranular dissolution pores (P_3) are connected by necking throat (T_2), Lithofacies C, Well TS5, 2,867.34 m (SEM); **(M)** intercrystalline pores (P_4) in the drill core, Lithofacies D, Well TD100, 3,823.41 m; **(N)** intercrystalline pores (P_4) are connected by the flaky throat (T_3), Lithofacies D, Well TD100, 3,823.41 m (PPL); **(O)** intercrystalline pores (P_4), Lithofacies D, Well TD110, 3,448.85 m (PPL); **(P)** intercrystalline pores (P_4) and flaky throat (T_3), Lithofacies D, Well TD110, 3,448.85 m (SEM).

4.1.2 Petrophysical property

Porosity and permeability are measured on 744 core plugs collected from 1) Lithofacies A ($n = 480$), 2) Lithofacies B ($n = 26$), 3) Lithofacies C ($n = 85$), and 4) Lithofacies D ($n = 153$). The average porosity of these four lithofacies is 2.7%, 2.6%, 7.0%, and 7.5%, respectively (Figure 4).

According to the Oil and Gas Industry Standard of the People's Republic of China (No. SY/T 6285-2011), Lithofacies A is characterized by ultra-low porosity and ultra-low permeability (Kralikova et al., 2016; Gao, 2019; Liu et al., 2022). The porosity distribution of Lithofacies A ranges from 2.00% to 8.90%, with an average value of 2.72%, mainly concentrated in 2.00%–4.00% (accounting for 93.21%) (Figure 4C). The permeability distribution of Lithofacies A ranges from less than .001 mD to 19.80 mD, with an

average value of .20 mD, mainly concentrated in the two intervals of less than .001 mD (account for 52.43%) and .001 mD–.01 mD (accounting for 33.48%) (Figure 4D). Lithofacies B is characterized by ultra-low porosity and ultra-low permeability. The porosity distribution of Lithofacies B ranges from 2.05% to 4.08%, with an average value of 2.59%, mainly concentrated in 2.00%–4.00% (account for 96.15%) (Figure 4C). The permeability of Lithofacies B is less than .0100 mD with an average of .0076 mD (Figure 4D).

Lithofacies C is characterized by low porosity and medium permeability, with porosity distribution ranging from 2.00% to 23.85%, with an average of 7.03% (Figure 4E). The permeability distribution of Lithofacies C ranges from less than .001 mD to 423.000 mD, with an average value of 29.260 mD, and it is distributed among various permeability intervals (Figure 4F). Lithofacies D is characterized by
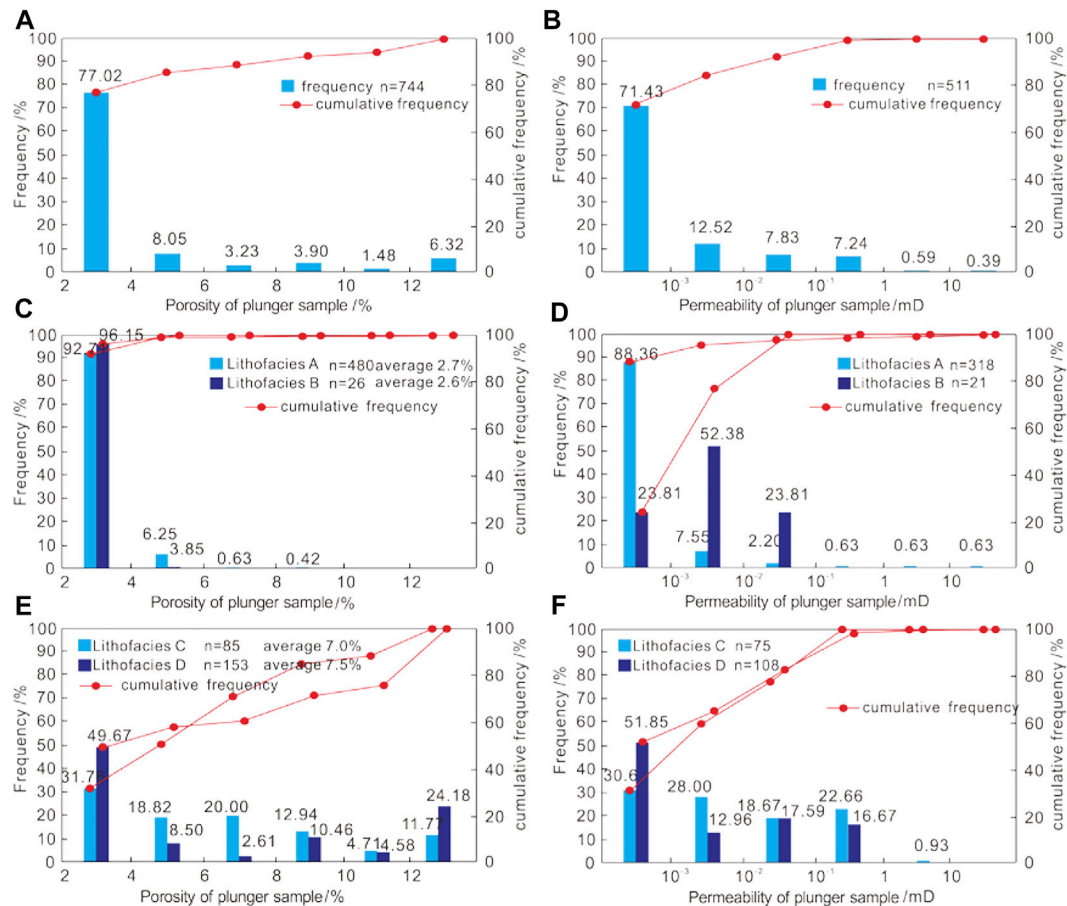
FIGURE 4
Petrophysical property of Feixianguan Formation tight oolitic reservoir.

low porosity and ultra-low permeability. The porosity of Lithofacies D ranges from 2.02% to 12.23%, with an average of 5.26%. They are distributed in all porosity intervals but mainly concentrated in the interval less than 8.00% (accounting for 88.46%) (Figure 4E). The permeability of Lithofacies D ranges from .0009 mD to 1.0200 mD, with an average value of .1700 mD, mainly concentrated in .0010 mD–1.0000 mD (accounting for 90.91%) (Figure 4F).

4.2 Pore-throat structure of different lithofacies

The pore-throat structure of a reservoir refers to the geometry, size, distribution, and connectivity of the pore body and throat. The pore-throat structure is the main controlling factor of the flow capability in a reservoir (Li et al., 2019b; Gu et al., 2020; Fan et al., 2022; Tang et al., 2022). In addition to the results discussed previously, we also carried out the pore-throat structure study using NMR, 3D-CT, and MICP data (Figure 5).
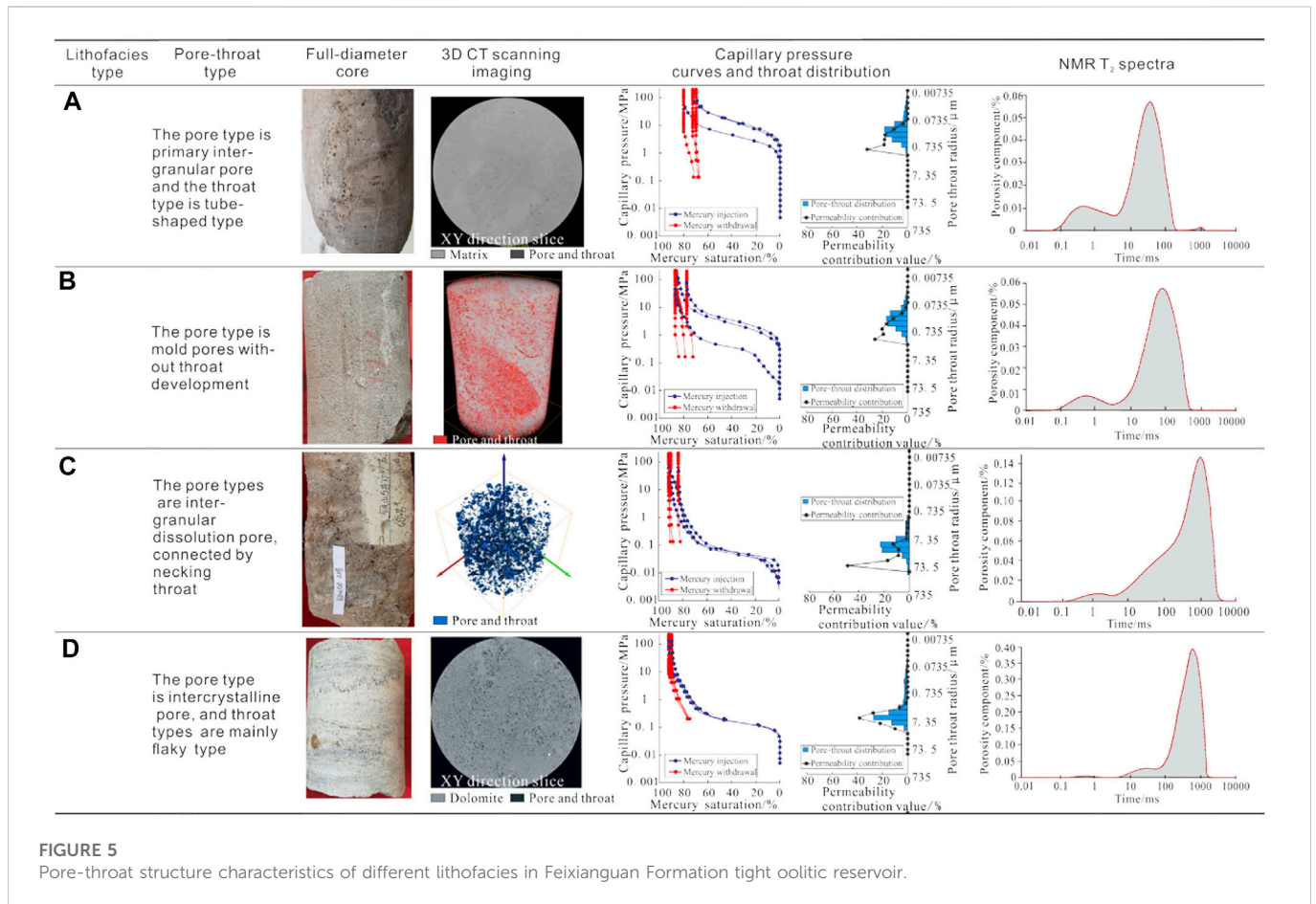
4.2.1 Lithofacies A

Lithofacies A is dominated by micropores, which are residual intergranular pores after cementation (Figure 5). The NMR T_2 spectrum reflects a bimodal pore-throat range of these samples.

NMR signals with the relaxation time between 0.1 ms and 1 ms represent smaller pore-throat size, and the corresponding porosity component is generally less than .015%. NMR signals with the relaxation time between 10 ms and 100 ms represent slightly larger pore-throat size, and the corresponding porosity component is generally less than .06%, indicating that the heterogeneity of pore-throat in Lithofacies A is strong and the contribution of slightly larger pore-throat to porosity is obviously greater than that of small pore-throat. Curves for Lithofacies A samples (n = 3) show high displacement pressures and low mercury saturation at any given pressure, indicating pore-throats are smaller and pores are less well connected.

4.2.2 Lithofacies B

Lithofacies B is dominated by mold pores ranging from 200 μm to 600 μm (Figure 5). The NMR T_2 spectrum reflects a bimodal pore-throat range of these samples. NMR signals with the relaxation time between 0.1 ms and 1 ms represent smaller mold pores, and the corresponding porosity component is generally less than .010%. NMR signals with the relaxation time between 10 ms and 500 ms represent larger mold pore, and the corresponding porosity component is generally greater than .05%, indicating that the heterogeneity of Lithofacies B is relatively weak and the contribution of larger mold pores to porosity is obviously greater

FIGURE 5
Pore-throat structure characteristics of different lithofacies in Feixianguan Formation tight oolitic reservoir.

than that of small mold pores. Curves for Lithofacies B samples ($n = 3$) show high displacement pressure and low mercury saturation at any given pressure, indicating mold pores are smaller and pores are less well connected.

4.2.3 Lithofacies C

Lithofacies C is dominated by macropores and small vugs, which are identified as intergranular dissolution pores and enlarged vugs by further dissolution (Figure 5). The NMR T_2 spectrum reflects a unimodal pore-throat range, indicating that the difference between the pore diameter and throat diameter is very small. NMR signals with the relaxation time greater than 100 ms represent larger pore-throat size, and the porosity component corresponding to these pore-throats is generally greater than .06%, indicating that the heterogeneity of pore-throats is weak. Also, the range of pore-throat radius also shows that the heterogeneity is weak. The large, well-connected pores and throats of Lithofacies C samples ($n = 3$) are indicated by low displacement pressures and the high mercury saturation at low injection pressures (.05 MPa–0.1 MPa). The broad, relatively flat plateaus between 0% and 70% mercury saturation suggest that about 70% of the pore volume is accessed by throats with an effective radius between 6 μm and 165 μm. The contribution of permeability mainly comes from the pore-throat with the radius greater than 15 μm.
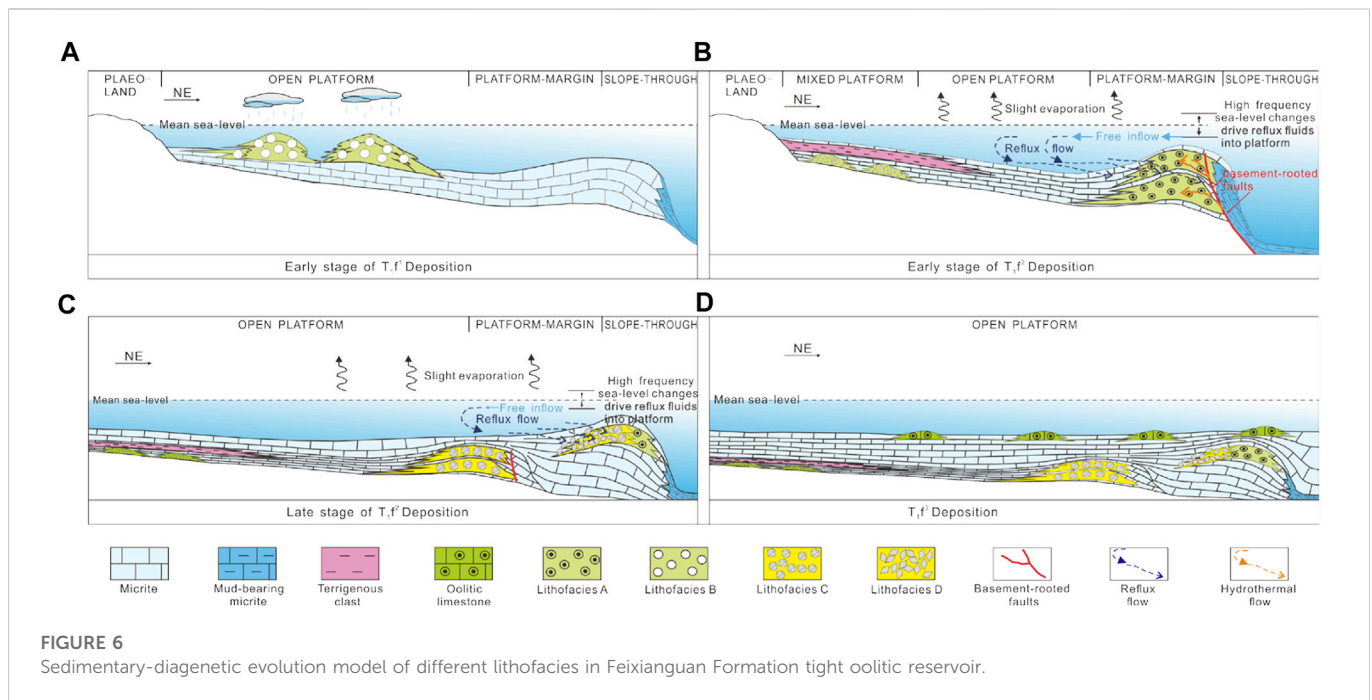
4.2.4 Lithofacies D

Lithofacies D is dominated by micropores, which are intercrystalline pores formed by intense dolomitization (Figure 5).

The NMR T_2 spectrum reflects a unimodal pore-throat range, indicating that the difference between the pore diameter and throat diameter is very small (Wang et al., 2019). NMR signals with the relaxation time between 100 ms and 1,000 ms represent a large pore-throat range, and the corresponding porosity component is generally greater than .10%, indicating that the heterogeneity of Lithofacies D is weak. Also, the range of pore-throat radius shows that the heterogeneity is weak. The large, well-connected pores and throats of Lithofacies D samples ($n = 3$) are indicated by low displacement pressure and high mercury saturation at relatively low injection pressures (.1M Pa–.5 MPa). The broad, relatively flat plateaus between 0% and 70% mercury saturation suggest that about 70% of the pore volume is accessed by throats with an effective radius between 1 μm and 147 μm. The contribution of permeability mainly comes from the pore-throat with the radius between 3 μm and 40 μm.

4.3 Origin of different lithofacies

4.3.1 Controlling factor of sedimentation

Whether the facies are deposited with platform-margin oolitic shoal or the open platform oolitic shoal, the porous sediments formed in the relatively high-energy environment are the most original material basis for reservoir rock (Tan et al., 2012; Mahmud et al., 2020). Early Triassic transgression led to a rapid sea-level rise in the study area during the early stage of T_1f^1 deposition. Because the landform is high in southwest and low in northeast (Xing et al.,

FIGURE 6
Sedimentary-diagenetic evolution model of different lithofacies in Feixianguan Formation tight oolitic reservoir.

2017; Ngene et al., 2022; Xia et al., 2022), at this time, the open platform landform highland is in the advantageous position of sedimentary oolitic shoals. Since the top of the oolitic shoals are close to the sea level, the oolitic shoals are susceptible to meteoric freshwater (Figure 6A). With the gradual decline in sea level and the increase in terrigenous debris input, the sedimentary process of oolitic shoals in the open platform stopped (Figure 6B). At this time, the platform-margin is near the wave base level, forming thick oolitic shoals due to high energy. After the formation of oolitic shoals on the platform margin, it is beneficial to forming a barrier environment behind the shoals (Figure 6C). As the sediments continuously filled the trough during T_1f^1–T_1f^2 deposition, the platform margin gradually moves to the trough. The barrier environment behind the shoals can be formed multiple times during this period. The whole study area evolved into an open platform, and the difference in sedimentary geomorphology disappeared, which is not conducive to inducing constructive diagenesis (Figure 6D).

4.3.2 Controlling factor of diagenesis
4.3.2.1 Fabric-selective dissolution

The exploration experience of oolitic reservoirs around the world indicates that fabric-selective dissolution is involved in the reservoir-forming process, such as Kangan Formation (Tavakoli et al., 2011; Enayati-Bidgoli et al., 2014; Rahimpour-Bonab et al., 2014) in South Pars gas field of the Persian Gulf Basin, Iran, Dalan Formation (Esrafili-Dizaji and Rahimpour-Bonab, 2013) in Zagros area, Messinian stage of the Neogene Miocene in Southeast Spain (Goldstein et al., 2013), and Arab Formation of the Jurassic in Balal Oilfield, Iran (Ebrahim et al., 2018). Lithofacies B is developed in the southwest of the study area, which is characterized by mold pores and multi-stage calcite cement. This phenomenon is strong evidence for the fabric-selective dissolution of the aragonite grains (Moore, 2001; Qie et al., 2021). The southwest part of the study area is close to the paleo-land. Under this background, the depth of seawater in the southwest of the study

area is less than that of other parts of the study area. The sedimentary environment of this area is relatively open, and the microscopic characteristics show that it is not affected by dolomitization. The ooids are formed continuously in the turbulent seawater of the submarine paleogeomorphic highland and then deposited, and the ooids are cemented by two-stage sparry calcite. When this area is located in the highstand system tract, the relative decline in the sea level and the vertical accretion of oolitic shoal in the open platform lead to be exposed beyond the sea level. Because of the unstable chemical properties and large specific surface area of aragonite ooids, fabric-selective dissolution is triggered by meteoric freshwater leaching during the syngenetic stage, while calcite cement is preserved because of its stable chemical properties and small specific surface area (Figure 6).

4.3.2.2 Dolomitization

The mechanism interpreted for dolomitization of Feixianguan oolitic dolostone mainly focuses on Eastern Kaijiang–Liangping Trough, including marine-meteoric mixing-zone (Yang et al., 2006), reflux (Jiang et al., 2013; Gu et al., 2020), thermal convection (Huang et al., 2011), or buried (Zheng et al., 2008) model. However, the marine-meteoric mixing-zone model has been questioned for its validity by academia (Hardie, 1987; Machel and Burton, 1994; Luczaj, 2006; Li et al., 2020), and the thermal-convection model seems relatively idealized. In terms of significant difference in the sedimentary environment between Eastern and Western Kaijiang–Liangping Trough, few studies suggest that hydrothermal brine and seepage-reflux brine are responsible for dolomitization in the platform margin of Western Kaijiang–Liangping Trough (Wang et al., 2018; Li et al., 2021a; Li et al., 2021b; Gu et al., 2021). For a long time, the contribution of dolomitization to carbonate reservoir formation has been controversial, and three main viewpoints have been proposed. First, dolomitization has limited contribution to the reservoir space; second, dolomitization only forms the dolomite framework to preserve primary pores; third, saddle dolomite
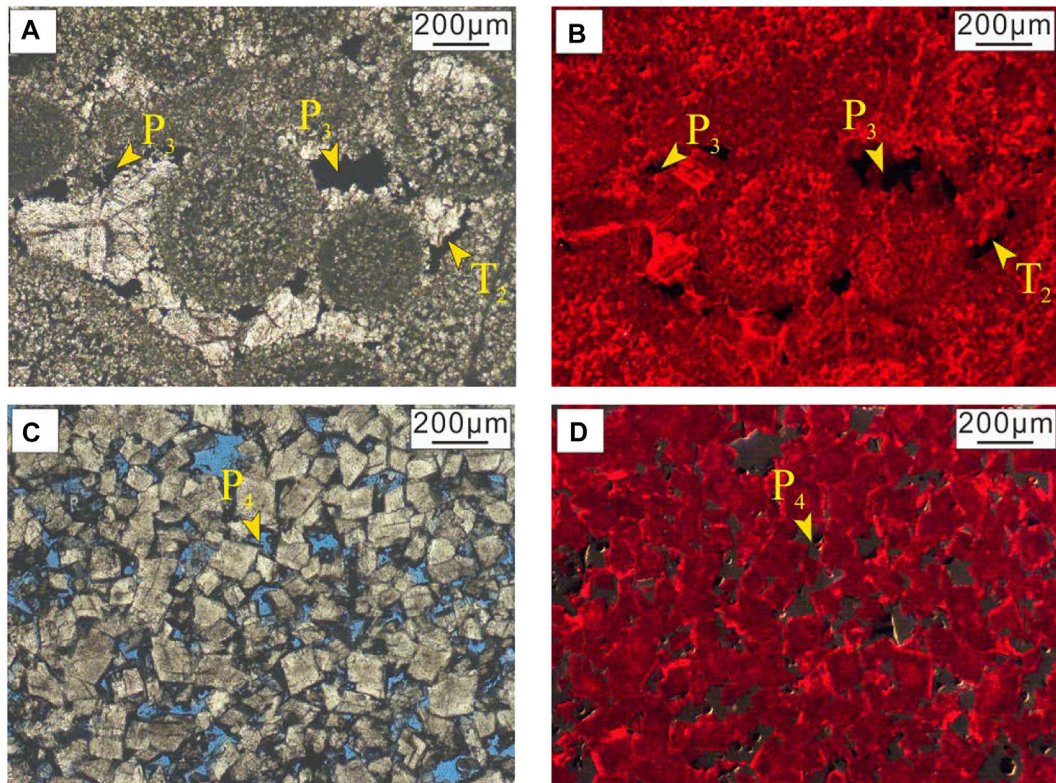
FIGURE 7
CL characteristics of Lithofacies C and D in Feixianguan Formation tight oolitic reservoir.

directly precipitated from dolomitization fluid blocks the reservoir space formed by other diagenesis processes (Shen et al., 2016; Zhao et al., 2018; Zhou et al., 2021). There is no saddle dolomite and other minerals precipitated by dolomitization fluid in the oolitic reservoir. According to the proportion of dolomite in the oolitic reservoir, it can be considered that dolomitization is the key to the formation or preservation of the reservoir space in the study area from either the first or the second point of view. Therefore, it is necessary to re-evaluate the dolomitization model in the study area.

Based on petrological characteristics, no compaction deformation of ooid is observed in Lithofacies C and D in the study area. A shadowy outline of ooids and dolomite crystalline are observed to be relatively loose, and stylolite is not observed. In Lithofacies C, dolomitization is fabric-selective, and usually ooids and first-stage cements are preferentially dolomitized (Figure 3). Under CL (Figure 7), Lithofacies C and D are non-luminescent. The $\delta^{18}O$ values of Lithofacies C and D samples are lower than those of normal Triassic seawater (Allan and Wiggins, 1993; Yoshida and Santosh, 2020), which indicates that the aging effect causes negative oxygen isotope migration in all samples (Figure 8). The unique geochemical characteristics of REE make it record the information of diagenetic fluids and diagenetic environment. It is an important method to understand diagenetic fluids and their origin. The ΣREE in all samples is lower than 12×10^{-6}, which generally shows the characteristics of low REE content in marine carbonate rocks (Hu et al., 2010). All Lithofacies D samples are similar to marine limestone including Lithofacies A, showing high LREE content, low HREE content, large positive Ce anomaly, and large positive Y anomaly.
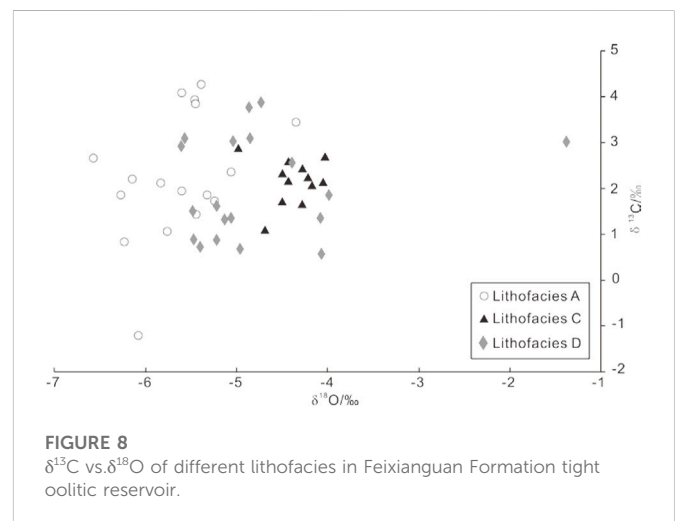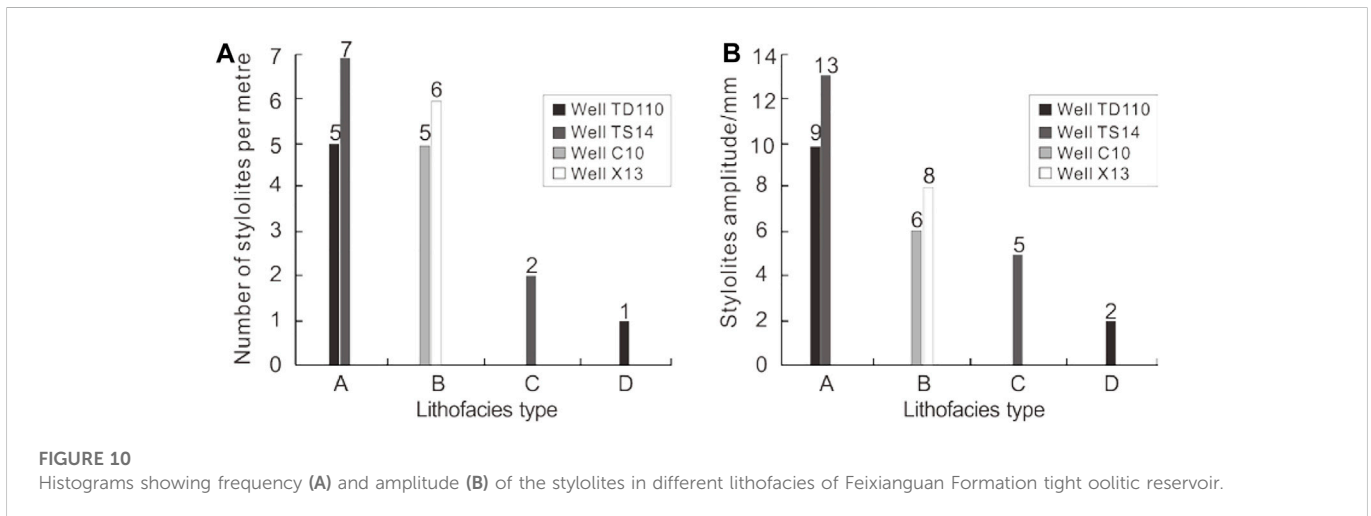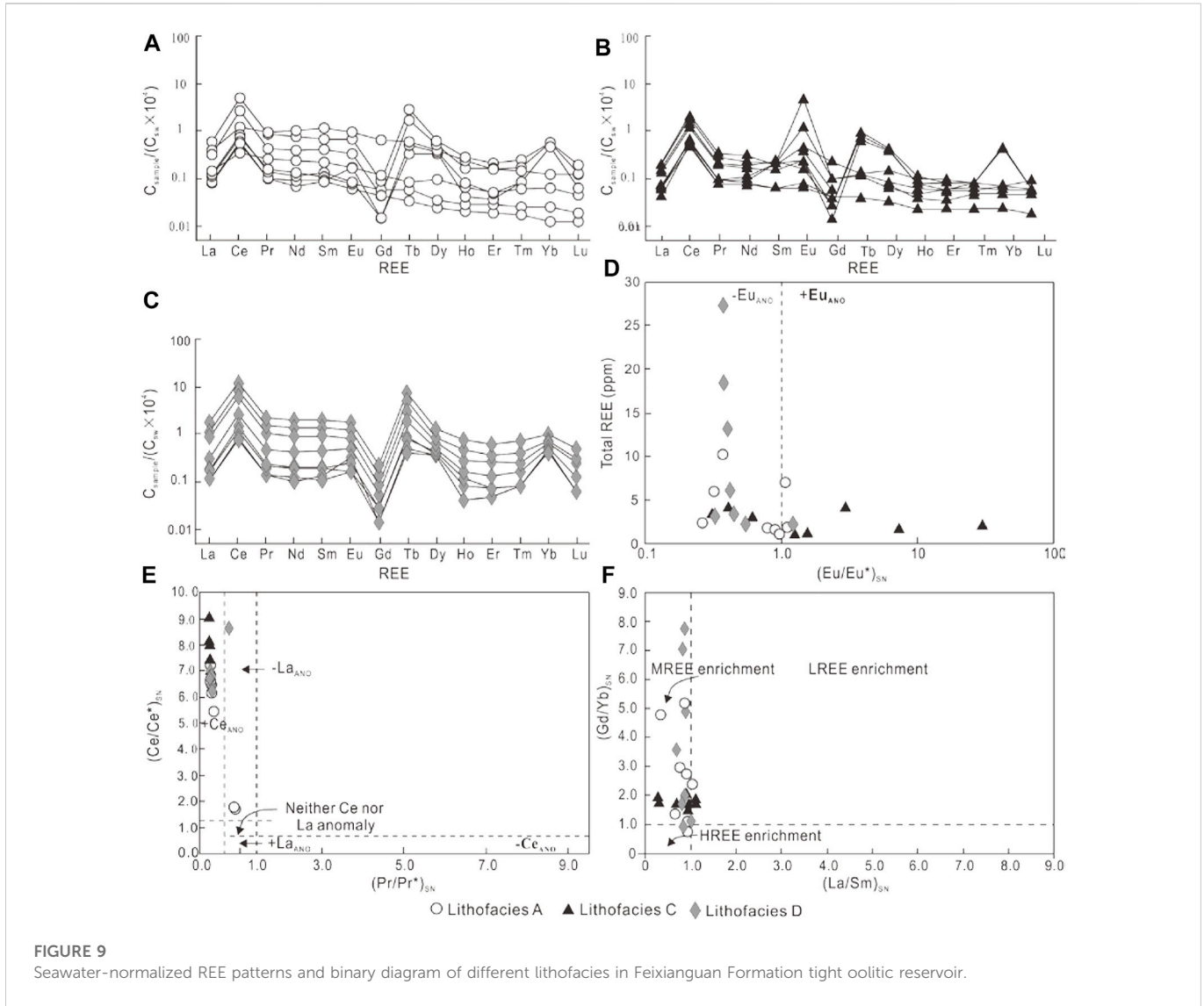

FIGURE 8
$\delta^{13}C$ vs.$\delta^{18}O$ of different lithofacies in Feixianguan Formation tight oolitic reservoir.

The first half of the segments show similar features of marine fluids; the second half of the segments for Lithofacies C samples show large fluctuation and are similar to saddle dolomite curves with remarkable positive Eu anomalies, which are related to hydrothermal activities (Hu et al., 2010; Jiang et al., 2016; Gu et al., 2019).

The petrological characteristics indicate that dolomitization occurred before large-scale compaction (Figure 3). Fabric-selective dolomitization and CL characteristics indicate that dolomitization of Lithofacies C and D occurs mostly before mineral stabilization, and the corresponding diagenetic environment is a submarine-shallow

FIGURE 9
Seawater-normalized REE patterns and binary diagram of different lithofacies in Feixianguan Formation tight oolitic reservoir.

FIGURE 10
Histograms showing frequency **(A)** and amplitude **(B)** of the stylolites in different lithofacies of Feixianguan Formation tight oolitic reservoir.

burial environment which is low in Fe or rich in Mn. Compared with Lithofacies A which has not undergone obvious dolomitization, the $\delta^{18}O$ of Lithofacies C and D shows a positive migration. It shows that

the enrichment of ^{18}O in reflux brine is caused by slight evaporation (Figure 8). Due to the barrier effect of platform-margin oolitic shoal during the deposition of $T_1f^1–T_1f^2$, penesaline seawater is formed by
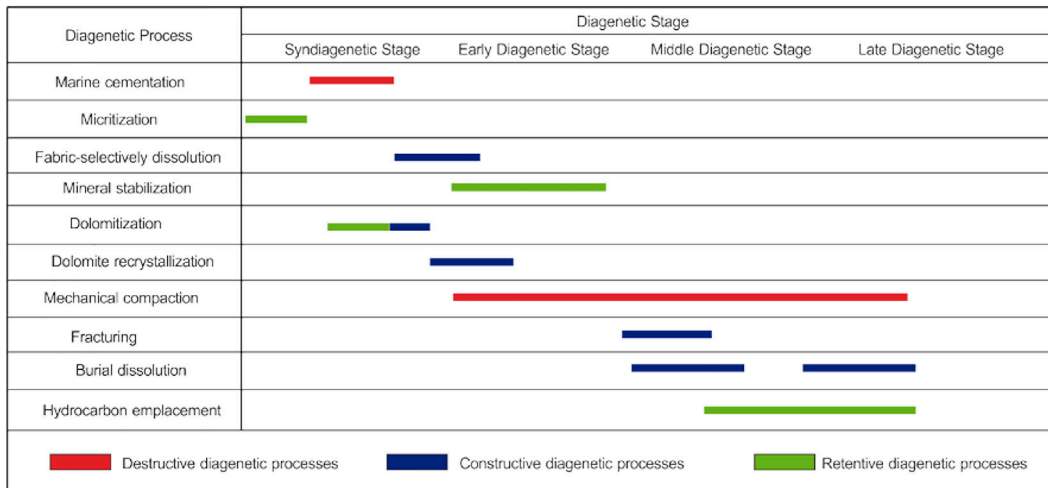
FIGURE 11
Paragenetic sequence of the diagenetic processes in Feixianguan Formation tight oolitic reservoir.
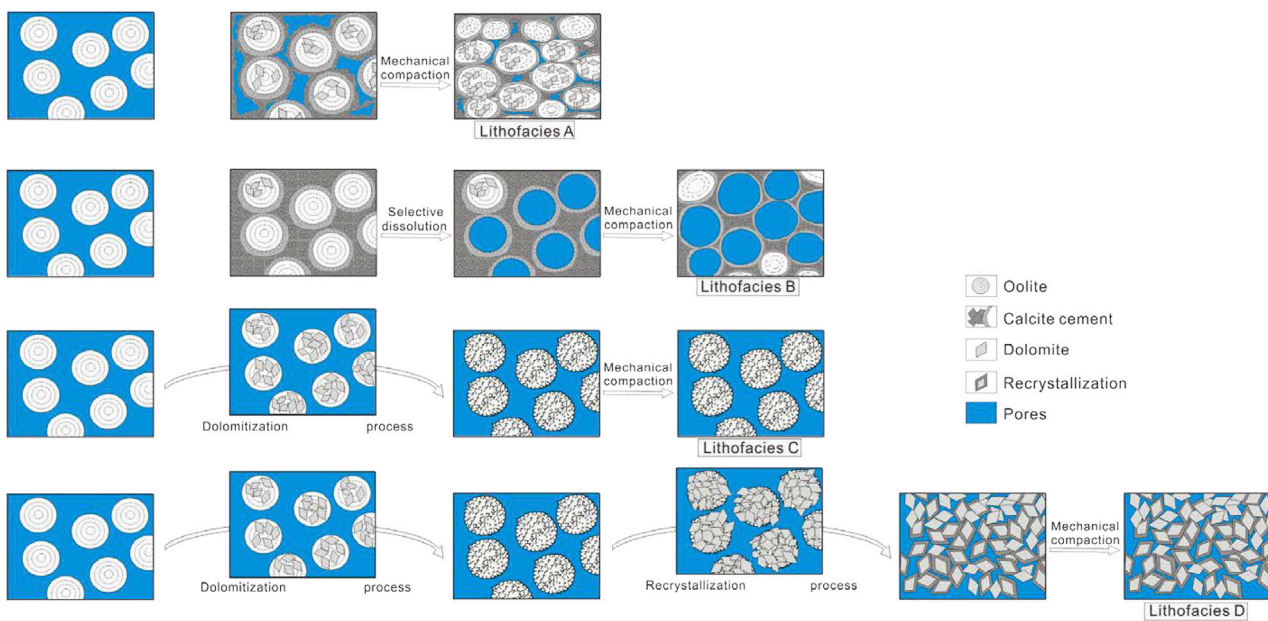

FIGURE 12
Diagenetic evolution of different lithofacies in Feixianguan Formation tight oolitic reservoir.

slight evaporation behind platform-margin oolitic shoals (Figures 6B, C). In the water–rock reaction process between hydrothermal fluids and oolitic limestone, Ca^{2+} in limestone is replaced by Eu^{2+} due to their equal valence and similar ionic radius; this leads to a positive Eu anomaly of Lithofacies C (Figure 9). The NW-trending basement faults of the Late Permian–Early Triassic provide migration channels for the upward migration of hydrothermal fluids (Wang et al., 2018). This study demonstrates that hydrothermal fluids also participate in the dolomitization of Lithofacies C (Figures 6A, B). Although the dolomitization mechanism of Lithofacies D is the same as that of C, the shadowy ooid outlines almost completely disappear and the crystal rim exhibits bright red (Figures 6C, D), indicating that the strong

recrystallization of dolomite occurs during the dolomitization process, which further improves the pore-throat structure of Lithofacies D.

4.3.2.3 Other diagenesis effects

Some other diagenesis effects may also have an impact on petrophysical properties of different lithofacies, but they do not play a decisive role in the origin of different lithofacies (Shan et al., 2021; Sun, 2023). The microscopic characteristics of different lithofacies and the development degree of stylolites show that the mechanical compaction has a destructive effect on the petrophysical properties of Lithofacies A and B but has little effect on Lithofacies C and D, indicating that dolomitization has

remarkable effect on improving the anti-compaction of reservoir lithofacies (Figure 10). During the syndiagenetic stage, micritization can be observed in many ooids, but the effect on rock fabric is extremely slight, which does not affect the differential evolution of lithofacies. During the middle-late diagenetic stage (Figure 11), accompanied by hydrocarbon charge and subsequent oxidative cracking of hydrocarbons, the organic acid or thermogenic sulfate reduction (TSR)-induced burial dissolution occurs in the oolitic reservoirs of the study area (Cai et al., 2014). The identified diagenetic processes that took place in different diagenetic stages are presented in Figure 12.

5 Conclusion

1) Four types of lithofacies exist in Feixianguan oolitic reservoirs of NE Sichuan Basin, namely, Lithofacies A, Lithofacies B, Lithofacies C, and Lithofacies D. The pore type of Lithofacies A is intergranular pores connected by the tube-shaped throat. Lithofacies B is characterized by mold pores, with the poorly developed throat. The pore type of Lithofacies C and D is intergranular dissolution pores connected by the necking throat and intercrystalline pore connected by the flaky throat, respectively.

2) Lithofacies A possesses small intergranular pores (100 μm–240 μm) that are connected by few tube-shaped throats with a bimodal pore-throat range. The heterogeneity of pore-throat in Lithofacies A is strong, and the contribution of slightly larger pore-throats to porosity is obviously greater than that of small pore-throats. Lithofacies B dominated by mold pores (200 μm–600 μm) also reflects a bimodal pore-throat range. Although the pore heterogeneity of Lithofacies B is weaker than that of Lithofacies A, there is no effective throat connection between the mold pores in Lithofacies B. Lithofacies C dominated by intergranular dissolution pores and vugs possess fairly larger pores (and vugs) that are well connected by large throats with a fairly narrow pore-throat size range. The heterogeneity of pore-throat in Lithofacies C is weak. The pore-throat structure of Lithofacies D is very similar to that of Lithofacies C, but the heterogeneity is obviously much weaker.

3) On the basis of oolitic shoal deposition, the main factors of diagenesis controlling the origin of different lithofacies are fabric-selective dissolution triggered by meteoric freshwater and dolomitization triggered by dolomitization fluids. The origin of Lithofacies B is dominated by meteoric freshwater leaching. The origin of Lithofacies C is not influenced by meteoric freshwater leaching but formed by the effect of seepage reflux and hydrothermal dolomitization fluids. The origin of Lithofacies D is only controlled by seepage-reflux dolomitization. Some other diagenesis effects may also have an impact on petrophysical properties of different lithofacies, but they do not play a decisive role in the origin of different lithofacies.

Data availability statement

The original contributions presented in the study are included in the article/Supplementary Material; further inquiries can be directed to the corresponding author.

Author contributions

GR: experiments, data analysis, visualization, and writing—original draft. QQ: conceptualization, methodology, and supervision. QZ: project administration and supervision. YG: supervision and revising the manuscript. ZY: data analysis and revising the manuscript.

Conflict of interest

Author QZ was employed by PetroChina Southwest Oil and Gas Field CDB Operating Company. Authors YG and ZY were employed by PetroChina Southwest Oil and Gas Field Company.

The remaining authors declare that the research was conducted in the absence of any commercial or financial relationships that could be construed as a potential conflict of interest.

Publisher's note

All claims expressed in this article are solely those of the authors and do not necessarily represent those of their affiliated organizations, or those of the publisher, the editors, and the reviewers. Any product that may be evaluated in this article, or claim that may be made by its manufacturer, is not guaranteed or endorsed by the publisher.

References

Abraham-A, R. M., Taioli, F., and Nzekwu, A. I. (2022). Physical properties of sandstone reservoirs: Implication for fluid mobility. *Energy Geosci.* 3 (4), 349–359. doi:10.1016/j.engeos.2022.06.001

Akin, R. H., and Graves, R. W. (1969). Reynolds oolite of southern Arkansas. *AAPG Bull.* 53 (9), 1909–1922.

Allan, J. R., and Wiggins, W. D. (1993). Dolomite reservoirs: Geochemical techniques for evaluating origin and distribution. *AAPG Contin. Educ. Course Note Ser.* 36, 129. doi:10.1016/0920-4105(95)00034-8

Bliefnick, D. M., and Kaldi, J. G. (1996). Pore geometry: Control on reservoir properties, walker Creek field, columbia and lafayette counties, Arkansas. *AAPG Bull.* 80 (7), 1027–1044. doi:10.1306/64ED8C82-1724-11D7-8645000102C1865D

Cai, C. F., He, W. X., Jiang, L., Li, K. K., Xiang, L., and Jia, L. Q. (2014). Petrological and geochemical constraints on porosity difference between Lower Triassic sour- and sweet-gas carbonate reservoirs in the Sichuan Basin. *Mar. Pet. Geol.* 56, 34–50. doi:10.1016/j.marpetgeo.2014.04.003

Deng, K. (1992). Formation and evolution of Sichuan Basin and domains oil and gas exploration. *Nat. Gas. Ind.* 12 (5), 7–13.

Ebrahim, S., Abdolhossien, A., Ali, K., Mohsen, S., and Seyed Mohammad, Z. (2018). Diagenetic and depositional impacts on the reservoir quality of the upper jurassic Arab Formation in the balal oilfield, offshore Iran. *Acta Geol. Sin. Engl. Ed.* 92 (4), 1523–1543. doi:10.1111/1755-6724.13641

Enayati-Bidgoli, A. H., Rahimpour-Bonab, H., and Mehrabi, H. (2014). Flow unit characterisation in the Permian-Triassic carbonate reservoir succession at South Pars Gasfield, offshore Iran. *J. Petroleum Geol.* 37 (3), 205–230. doi:10.1111/jpg.12580

Enos, P., and Sawatsky, L. H. (1981). Pore networks in Holocene carbonate sediments. *J. Sediment. Petrology* 51 (3), 961–985. doi:10.1306/212F7DF1-2B24-11D7-8648000102C1865D

Esrafili-Dizaji, B., and Rahimpour-Bonab, H. (2013). A review of permo-triassic reservoir rocks in the Zagros area, SW Iran: Influence of the Qatar-fars arch. *J. Petroleum Geol.* 36 (3), 257–279. doi:10.1111/jpg.12555

Esrafili-Dizaji, B., and Rahimpour-Bonab, H. (2014). Generation and evolution of oolitic shoal reservoirs in the Permo-Triassic carbonates, the South Pars Field, Iran. *Facies* 60 (4), 921–940. doi:10.1007/s10347-014-0414-4

Fairchild, J. J., and Spiro, B. (1987). Petrological and isotopic implications of some contrasting Late Precambrian carbonates, NE Spitsbergen. *Sedimentology* 34 (6), 973–989. doi:10.1111/j.1365-3091.1987.tb00587.x

Fan, C. H., Li, H., Qin, Q. R., He, S., and Zhong, C. (2020). Geological conditions and exploration potential of shale gas reservoir in Wufeng and Longmaxi Formation of southeastern Sichuan Basin, China. *J. Petrol. Sci. Eng.* 191, 107138. doi:10.1016/j.petrol.2020.107138

Fan, C., Xie, H. B., Li, H., Zhao, S., Shi, X., Liu, J., et al. (2022). Complicated Fault characterization and its influence on shale gas preservation in the southern margin of the Sichuan Basin, China. *Lithosphere* 2022, 8035106. doi:10.2113/2022/8035106

Forstner, S. R., and Laubach, S. E. (2022). Scale-dependent fracture networks. *J. Struct. Geol.* 165, 104748. doi:10.1016/j.jsg.2022.104748

Gao, F. Q. (2019). Use of numerical modeling for analyzing rock mechanic problems in underground coal mine practices. *J. Min. Strata Control Eng.* 1 (1), 013004. doi:10.13532/j.jmsce.cn10-1638/td.2019.02.009

Goldstein, R. H., Franseen, E. K., and Lipinski, C. J. (2013). Topographic and sea level controls on oolite-microbialite-coralgal reef sequences: The terminal carbonate complex of southeast Spain. *AAPG Bull.* 97 (11), 1997–2034. doi:10.1306/06191312170

Granier, B. A. (1995). A sedimentological model of the Callovian oolite reservoir of the Villeperdue oil field, Paris Basin (France). *Pet. Geosci.* 1 (2), 145–150. doi:10.1144/petgeo.1.2.145

Gu, Y., Zhou, L., Jiang, Y., Jiang, C., Luo, M., and Zhu, X. (2019). A model of hydrothermal dolomite reservoir facies in Precambrian dolomite, Central Sichuan Basin, SW China and its geochemical characteristics. *Acta Geol. Sin. Engl. Ed.* 93 (1), 130–145. doi:10.1111/1755-6724.13770

Gu, Y., Jiang, Y., Qing, H., Feng, L., Feng, L., Fu, Y., et al. (2020). Reservoir characteristics, pore structure, and main controlling factors of oolitic shoal reservoir in Feixianguan Formation: A case study from eastern Kaijiang-Liangping Trough. *Arabian J. Geosciences* 13, 309. doi:10.1007/s12517-020-05286-x

Gu, Y., Jiang, Y., Lei, X., Chen, Z., Zhou, L., Fu, Y., et al. (2021). The major controlling factors and different oolitic shoal reservoir characteristics of the Triassic Feixianguan Formation, Eastern Longgang area, NE Sichuan Basin, SW China. *Acta Geol. Sin. Engl. Ed.* 95 (3), 895–908. doi:10.1111/1755-6724.14672

Guo, P., Yao, L. H., and Ren, D. S. (2016). Simulation of three-dimensional tectonic stress fields and quantitative prediction of tectonic fracture within the Damintun Depression, Liaohe Basin, northeast China. *J. Struct. Geol.* 86, 211–223. doi:10.1016/j.jsg.2016.03.007

Hao, F., Guo, T., Zhu, Y., Cai, X., Zou, H., and Li, P. (2008). Evidence for multiple stages of oil cracking and thermochemical sulfate reduction in the Puguang gas field, Sichuan Basin, China. *AAPG Bull.* 92, 611–637. doi:10.1306/01210807090

Hardie, L. A. (1987). Dolomitization: A critical view of some current views. *J. Sediment. Res.* 57 (1), 166–183. doi:10.1306/212F8AD5-2B24-11D7-8648000102C1865D

He, D. F., Li, D. S., Zhang, G. W., Zhao, L. Z., Fang, C., Lu, R. Q., et al. (2011). Formation and evolution of multi-cycle superposed Sichuan Basin, China. *Chin. J. Geol.* 46 (3), 589–606.

He, S., Qin, Q., Li, H., and Long, S. (2021). Influence of mineral compositions on shale pore development of Longmaxi Formation in the Dingshan area, southeastern Sichuan Basin, China. *Energy Fuels* 35 (13), 10551–10561. doi:10.1021/acs.energyfuels.1c01026

Hu, W., Chen, Q., Wang, X., and Cao, J. (2010). REE models for the discrimination of fluids in the formation and evolution of dolomite reservoirs. *Oil Gas Geol.* 31 (6), 810–818. doi:10.1016/S1876-3804(11)60008-6

Huang, S., Huang, Y., Lan, Y., and Huang, K. (2011). A comparative study on strontium isotope composition of dolomites and their coeval seawater in the Late Permian-Early Triassic, NE Sichuan Basin. *Acta Petrol. Sin.* 27 (12), 3831–3842.

Jiang, L., Cai, C. F., Worden, R. H., Li, K. K., and Xiang, L. (2013). Reflux dolomitization of the upper permian changxing formation and the lower triassic Feixianguan Formation, NE Sichuan Basin, China. *Geofluids* 13 (2), 232–245. doi:10.1111/gfl.12034

Jiang, Y., Tao, Y., Gu, Y., Wang, J., Qiang, Z., Jiang, N., et al. (2016). Hydrothermal dolomitization in dengying formation, gaoshiti-moxi area, Sichuan Basin, SW China. *Petroleum Explor. Dev.* 43 (1), 54–64. doi:10.1016/S1876-3804(16)30006-4

Jin, M. D., Li, B. S., Zhu, X., Dai, L. C., Jiang, Z. L., Wu, H., et al. (2020). Characteristics and main controlling factors of reservoirs in the fourth member of Sinian Dengying Formation in Yuanba and its peripheral area, northeastern Sichuan Basin, SW China. *Petroleum Explor. Dev.* 47 (6), 1172–1182. doi:10.1016/S1876-3804(20)60127-1

Kang, H. P. (2021). Temporal scale analysis on coal mining and strata control technologies. *J. Min. Strata Control Eng.* 3 (1), 013538. doi:10.13532/j.jmsce.cn10-1638/td.20200814.001

Kawabe, I., Toriumi, T., Ohta, A., and Miura, N. (1998). Monoisotopic REE abundances in seawater and the origin of seawater tetrad effect. *Geochem J.* 32 (4), 213–229. doi:10.2343/geochemj.32.213

Kiani, S., Jafari, S., Apourvari, S. N., and Mehrjoo, H. (2021). Simulation study of wormhole formation and propagation during matrix acidizing of carbonate reservoirs using a novel *in-situ* generated hydrochloric acid. *Adv. Geo-Energy Res.* 5 (1), 64–74. doi:10.46690/ager.2021.01.07

Kralikova, S., Vojtko, R., Hok, J., Fugenschuh, B., and Kovac, M. (2016). Low-temperature constraints on the Alpine thermal evolution of the Western Carpathian basement rock complexes. *J. Struct. Geol.* 91, 144–160. doi:10.1016/j.jsg.2016.09.006

Li, W. P., Liu, S. F., Wang, Y., Qian, T., and Gao, T. J. (2017). Duplex thrusting in the South Dabashan arcuate belt, central China. *J. Struct. Geol.* 103, 120–136. doi:10.1016/j.jsg.2017.09.007

Li, H., Li, Z. Q., Long, W., Wan, S. S., Ding, S., Wang, S. Z., et al. (2019a). Vertical configuration of Sichuan Basin and its superimposed characteristics of the prototype basin. *J. Chengdu Unniversity Technol. Sci. Technol. Ed.* 46 (3), 257–267. doi:10.3969/j.issn.1671-9727.2019.03.01

Li, H., Tang, H. M., Qin, Q. R., Zhou, J. L., Qin, Z. J., Fan, C. H., et al. (2019b). Characteristics, formation periods and genetic mechanisms of tectonic fractures in the tight gas sandstones reservoir: A case study of xujiahe Formation in YB area, Sichuan Basin, China. *J. Petrol. Sci. Eng.* 178, 723–735. doi:10.1016/j.petrol.2019.04.007

Li, H., Wang, Q., Qin, Q. R., and Ge, X. Y. (2021a). Characteristics of natural fractures in an ultradeep marine carbonate gas reservoir and their impact on the reservoir: A case study of the maokou Formation of the jls structure in the Sichuan Basin, China. *Energy & Fuels* 35 (16), 13098–13108. doi:10.1021/acs.energyfuels.1c01581

Li, H., Peng, R., Du, W. S., Li, X. P., and Zhang, N. B. (2021b). Experimental study on structural sensitivity and intervention mechanism of mechanical behavior of coal samples. *J. Min. Strata Control Eng.* 3 (4), 043012. doi:10.13532/j.jmsce.cn10-1638/td.20210820.001

Li, H., Qin, Q. R., Zhang, B. J., Ge, X. Y., Hu, X., Fan, C. H., et al. (2020). Tectonic fracture formation and distribution in ultradeep marine carbonate gas reservoirs: A case study of the maokou Formation in the jiulongshan gas field, Sichuan Basin, southwest China. *Energy & Fuels* 34 (11), 14132–14146. doi:10.1021/acs.energyfuels.0c03327

Li, H., Zhou, J. L., Mou, X. Y., Guo, H. X., Wang, X. X., An, H. Y., et al. (2022). Pore structure and fractal characteristics of the marine shale of the longmaxi Formation in the changning area, southern Sichuan Basin, China. *Front. Earth Sci.* 10, 1018274. doi:10.3389/feart.2022.1018274

Li, J., Li, H., Yang, C., Wu, Y. J., Gao, Z., and Jiang, S. L. (2022). Geological characteristics and controlling factors of deep shale gas enrichment of the wufeng-longmaxi Formation in the southern Sichuan Basin, China. *Lithosphere* 2022, 4737801. doi:10.2113/2022/4737801

Li, K., George, S. C., Cai, C. F., Zhang, X., and Tan, X. (2020). Comparison of differential diagenesis of two oolites on the Lower Triassic platform margin, NE Sichuan Basin: Implications for the co-evolution of rock structure and porosity. *Mar. Petroleum Geol.* 119, 104485. doi:10.1016/j.marpetgeo.2020.104485

Li, Y., Zhou, D., Wang, W., Jiang, T., and Xue, Z. (2020). Development of unconventional gas and technologies adopted in China. *Energy Geosci.* 1 (1-2), 55–68. doi:10.1016/j.engeos.2020.04.004

Li, H. (2022). Research progress on evaluation methods and factors influencing shale brittleness: A review. *Energy Rep.* 8, 4344–4358. doi:10.1016/j.egyr.2022.03.120

Liu, S., Li, Z., Sun, W., Deng, B., Luo, Z., Wang, G., et al. (2011). Basin geological features of superimposed basin and hydrocarbon accumulation in Sichuan Basin, China. *Chin. J. Geol.* 46 (1), 233–257. doi:10.3969/j.issn.0563-5020.2011.01.019

Liu, C., Zhang, L., Li, Y., Liu, F., Martyushev, D. A., and Yang, Y. (2022). Effects of microfractures on permeability in carbonate rocks based on digital core technology. *Adv. Geo-Energy Res.* 6 (1), 86–90. doi:10.46690/ager.2022.01.07

Luczaj, J. A. (2006). Evidence against the dorag (mixing-zone) model for dolomitization along the Wisconsin arch? A case for hydrothermal diagenesis. *AAPG Bull.* 90 (11), 1719–1738. doi:10.1306/01130605077

Machel, H. G., and Burton, E. A. (1994). Golden grove dolomite, Barbados: Origin from modified seawater. *J. Sediment. Res.* 64 (4), 741–751. doi:10.1306/D4267EAB-2B26-11D7-8648000102C1865D

Mahmud, H., Hisham, M., Mahmud, M., Leong, V., and Shafiq, M. (2020). Petrophysical interpretations of subsurface stratigraphic correlations, Baram Delta, Sarawak, Malaysia. *Energy Geosci.* 1 (3-4), 100–114. doi:10.1016/j.engeos.2020.04.005

Makhloufi, Y., Collin, P., Bergerat, F., Casteleyn, L., Claes, S., David, C., et al. (2013). Impact of sedimentology and diagenesis on the petrophysical properties of a tight oolitic carbonate reservoir: The case of the Oolithe Blanche Formation (Bathonian, Paris Basin, France). *Mar. Petroleum Geol.* 48, 323–340. doi:10.1016/j.marpetgeo.2013.08.021

Moore, C. H. (2001). *Carbonate reservoirs: Porosity evolution and diagenesis in a sequence stratigraphic framework*. Amsterdam: Elsevier, 444.

Morad, S., Al Suwaidi, M., Mansurbeg, H., Morad, D., Ceriani, A., Paganoni, M., et al. (2019). Diagenesis of a limestone reservoir (lower cretaceous), abu dhabi, united Arab emirates: Comparison between the anticline crest and flanks. *Sediment. Geol.* 380, 127–142. doi:10.1016/j.sedgeo.2018.12.004

Ngene, T., Mukhopadhyay, M., and Ampana, S. (2022). Reconnaissance investigation of geothermal resources in parts of the Middle Benue Trough, Nigeria using remote sensing and geophysical methods. *Energy Geosci.* 3 (4), 360–371. doi:10.1016/j.engeos.2022.06.002

Palermo, D., Aigner, T., Geluk, M., Poeppelreiter, M., and Pipping, K. (2008). Reservoir potential of a lacustrine mixed carbonate/siliciclastic gas reservoir: The lower triassic rogenstein in The Netherlands. *J. Petroleum Geol.* 31 (1), 61–96. doi:10.1111/j.1747-5457.2008.00407.x

Qi, L., Carr, T. R., and Goldstein, R. H. (2007). Geostatistical three-dimensional modeling of oolite shoals, St. Louis Limestone, southwest Kansas. *AAPG Bull.* 91 (1), 69–96. doi:10.1306/08090605167

Qiao, Z., Janson, X., Shen, A., Zheng, J., Zeng, H., and Wang, X. (2016). Lithofacies, architecture, and reservoir heterogeneity of tidal-dominated platform marginal oolitic shoal: An analogue of oolitic reservoirs of lower triassic Feixianguan Formation, Sichuan Basin, SW China. *Mar. Petroleum Geol.* 76, 290–309. doi:10.1016/j.marpetgeo.2016.05.030

Qie, L., Shi, Y. N., and Liu, J. G. (2021). Experimental study on grouting diffusion of gangue solid filling bulk materials. *J. Min. Strata Control Eng.* 3 (2), 023011. doi:10.13532/j.jmsce.cn10-1638/td.20201111.001

Rahimpour-Bonab, H., Enayati-Bidgoli, A. H., and Navidtalab, A. (2014). Appraisal of intra reservoir barriers in the permo-triassic successions of the central Persian Gulf, offshore Iran. *Geol. Acta* 12 (1), 87–107. doi:10.1344/105.000002076

Ren, G., Qin, Q., Qin, Z., Guo, Y., and Ye, Z. (2022). Effects of diagenesis on quality of deep dolomite reservoirs:A case study of the Upper Cambrian Xixiangchi Formation in the eastern Sichuan Basin, China. *Front. Earth Sci.* 10, 984463. doi:10.3389/feart.2022.984463

Schmoker, J., and Hester, T. (1986). Porosity of the miami limestone (late pleistocene), lower Florida keys. *J. Sediment. Petrology* 56 (5), 629–634. doi:10.1306/212F89F4-2B24-11D7-8648000102C1865D

Shan, S. C., Wu, Y. Z., Fu, Y. K., and Zhou, P. H. (2021). Shear mechanical properties of anchored rock mass under impact load. *J. Min. Strata Control Eng.* 3 (4), 043034. doi:10.13532/j.jmsce.cn10-1638/td.20211014.001

Shen, A., Zheng, J., Chen, Y., Ni, X., and Huang, L. (2016). Characteristics, origin and distribution of dolomite reservoirs in lower-middle cambrian, tarim basin, NW China. *Petroleum Explor. Dev.* 43 (3), 375–385. doi:10.1016/S1876-3804(16)30044-1

Shen, W., Li, X., Cihan, A., Lu, X., and Liu, X. (2019). Experimental and numerical simulation of water adsorption and diffusion in shale gas reservoir rocks. *Adv. Geo-Energy Res.* 3 (2), 165–174. doi:10.26804/ager.2019.02.06

Shields, G., and Stile, P. (2001). Diagenetic constraints on the use of cerium anomalies as palaeoseawater redox proxies: An isotopic and REE study of Cambrian phosphorites. *Chem. Geol.* 175 (1-2), 29–48. doi:10.1016/S0009-2541(00)00362-4

Sun, Z. M. (2023). Superimposed hydrocarbon accumulation through multi-source and multi-stage evolution in the cambrian xixiangchi group of eastern Sichuan Basin: A case study of the pingqiao gas-bearing anticline. *Energy Geosci.* 4 (1), 131–142. doi:10.1016/j.engeos.2022.09.001

Swirydczuk, K. (1988). Mineralogical controlon porosity type in upper jurassic smackover ooid grainstones, southern Arkansas and northern Louisiana. *J. Sediment. petrology* 58 (2), 339–347. doi:10.1306/212F8D8C-2B24-11D7-8648000102C1865D

Tan, X., Zhao, L., Luo, B., Jiang, X., Cao, J., Liu, H., et al. (2012). Comparison of basic features and origins of oolitic shoal reservoirs between carbonate platform interior and platform margin locations in the Lower Triassic Feixianguan Formation of the Sichuan Basin, southwest China. *Petroleum Sci.* 9, 417–428. doi:10.1007/s12182-012-0229-2

Tang, Y., Tan, S. H., Wang, R. F., Wang, H., Xia, C. M., and Chen, K. Y. (2022). Analysis of tight oil accumulation conditions and prediction of sweet spots in ordos basin: A case study. *Energy Energy Geosci.* 3 (4), 417–426. doi:10.1016/j.engeos.2021.09.002

Tavakoli, V., Rahimpour-Bonab, H., and Esrafili-Dizaji, B. (2011). Diagenetic controlled reservoir quality of South Pars gas field, an integrated approach. *Comptes rendus - Géoscience* 343 (1), 55–71. doi:10.1016/j.crte.2010.10.004

Wang, Q., and Jin, Z. (2002). Superimposed basin and oil-gas formation and accumulation. *Chin. Basic Sci.* 6, 4–7. doi:10.3969/j.issn.1009-2412.2002.06.001

Wang, Z., Jiang, C., Jiang, Y., Zhang, J., and Gu, Y. (2018). Distribution patterns and controlling factors for reservoir characteristic difference of oolitic shoals, Feixian'guan Formation, eastern Longgang area, SW China. *Arabian J. Geosciences* 11, 751. doi:10.1007/s12517-018-4082-5

Wang, X., Yin, H., Zhao, X., Li, B., and Yang, Y. (2019). Microscopic remaining oil distribution and quantitative analysis of polymer flooding based on CT scanning. *Adv. Geo-Energy Res.* 3 (4), 448–456. doi:10.26804/ager.2019.04.10

Wei, G., Yang, W., Xie, W., Jin, H., Su, N., Sun, A., et al. (2018). Accumulation modes and exploration domains of Sinian-Cambrian natural gas in Sichuan Basin. *Acta Pet. Sin.* 39 (12), 1317–1327. doi:10.7623/syxb201812001

Xia, D. L., Wu, Y., Zou, M., Xia, D. D., and Pang, W. (2022). Quality characterization of tight sandstone reservoirs in the honghe oilfield, ordos basin, central China. *Energy Geosci.* 3 (4), 444–452. doi:10.1016/j.engeos.2021.07.001

Xing, F., Lu, Y., Guo, T., Li, S., Hou, M., Hu, H., et al. (2017). Sedimentary texture diversity of different carbonate platform margins and it its significance for petroleum exploration: A case study of carbonate platform margins in feixianguan period of the early triassic, NE Sichuan Basin, China. *Acta Petrol. Sin.* 33 (4), 1305–1316.

Yang, X., Zhao, W., Cao, H., Yang, Y., Zhang, B., and Tao, S. (2006). Fomation and distribution of Triassic Feixianguan oolitic bank favorable reservoir in the NE Sichuan Basin. *Petroleum Explor. Dev.* 33 (1), 17–21. doi:10.3321/j.issn:1000-0747.2006.01.004

Yoshida, M., and Santosh, M. (2020). Energetics of the solid earth: An integrated perspective. *Energy Geosci.* 1 (1-2), 28–35. doi:10.1016/j.engeos.2020.04.001

Zhao, W., Shen, A., Qiao, Z., Pan, L., Hu, A., and Zhang, J. (2018). Genetic types and distinguished characteristics of dolomite and the origin of dolomite reservoirs. *Petroleum Explor. Dev.* 45 (6), 983–997. doi:10.1016/s1876-3804(18)30103-4

Zheng, R., Geng, W., Zheng, C., Li, S., Li, G., Luo, P., et al. (2008). Genesis of dolostone reseriyoir of Feixianguan Formation in lower triassic of northeast Sichuan Basin. *Acta Pet. Sin.* 29 (6), 815–821. doi:10.3321/j.issn:0253-2697.2008.06.005

Zhou, Z., Wang, X., Yin, G., Yuan, S., and Zeng, S. (2016). Characteristics and Genesis of the (sinian) dengying formation reservoir in central sichuan, China. *J. Nat. Gas Sci. Eng.* 29, 311–321. doi:10.1016/j.jngse.2015.12.005

Zhou, J., Deng, H., Yu, Z., Guo, Q., Zhang, R., Zhang, J., et al. (2019). The Genesis and prediction of dolomite reservoir in reef-shoal of changxing formation-feixianguan Formation in Sichuan Basin. *J. Petroleum Sci. Eng.* 178, 324–335. doi:10.1016/j.petrol.2019.03.020

Zhou, Y., Jiang, Y., Liang, J., Gu, Y., Fu, Y., and Xiao, Y. (2021). Reservoir characteristics and major controlling factors of the cambrian xixiangchi formation, central Sichuan Basin, southwest China. *J. Energy Eng.* 147 (6), 04021051. doi:10.1061/(ASCE)EY.1943-7897.0000803

Zou, C., Xu, C., Wang, Z., Hu, S., Yang, G., Li, J., et al. (2011). Geological characteristics and forming conditions of the platform margin large reef-shoal gas province in the Sichuan Basin. *Petroleum Explor. Dev.* 38 (6), 641–651. doi:10.1016/s1876-3804(12)60001-9